

INTERSTELLAR H I SHELLS IDENTIFIED IN THE SETHI SURVEY

SHAUNA M. SALLMEN¹, ERIC J. KORPELA², BROOKE BELLEHUMEUR³, ELIZABETH M. TENNYSON⁴, KURT GRUNWALD¹,
CHEUK MAN LO⁵*Accepted by The Astronomical Journal*

ABSTRACT

Galactic H I (neutral hydrogen) shells are central to our understanding of the interstellar medium (ISM), which plays a key role in the development and evolution of galaxies, including our own. Several models involving supernovae and stellar winds have contributed to our broad understanding, but a complete, detailed picture remains elusive. To extend existing Galactic shell catalogs, we visually examined the SETHi (Search for Extraterrestrial H I) database to identify shell-like structures. This high-sensitivity 21-cm radio survey covering the Arecibo sky uniquely provides high-resolution data on shells at a wide range of Galactic latitudes. We present basic information (location, radial velocity, angular size, shape) for 74 previously unidentified H I shells. Due to limitations of coverage and data quality, and the biases inherent in search techniques, our catalog is not a complete sample of Galactic shells. We discuss the catalog completeness, and comment on the new shells' relationship with known interstellar structure as warranted. Unlike many previous catalogs, this sample is not biased towards expanding shells. Where possible we also estimate the kinematic distances, physical sizes, expansion velocities, and energies of these shells. Overall, they are relatively large and old, each the result of multiple supernovae. Unlike previous surveys, we do not find that the shells in our sample are preferentially aligned relative to the Galactic plane.

Keywords: ISM: general – ISM: bubbles – ISM: supernova remnants – radio lines: ISM – astronomical databases: catalogs

1. INTRODUCTION

The interstellar medium (ISM) plays a key role in the development and evolution of galaxies, including our own. The effects of generations of stars within the galactic ISM have produced a turbulent, multi-phase medium filled with complex interacting structures. Shells, bubble-like features, “chimneys” and “worms” were first identified in neutral hydrogen (H I) maps by Heiles (1979, 1984). These structures are driven by stellar winds and supernova (SN) explosions. These processes are responsible for redistributing energy and material throughout our galaxy, resulting in the formation of new generations of stars.

The physical state and evolution of these gas phases are likely explained (at least in part) by the three-phase model of McKee & Ostriker (1977), wherein random supernovae result in a turbulent ISM of hot, low-density gas surrounding warm and cold clouds. In the Galactic fountain model of Shapiro & Field (1976), hot gas rises out of the Galactic plane, cools, then falls back into the Galactic plane. Superbubbles (caused by clusters of supernovae) can break out of the Galactic plane providing a source of buoyant hot gas to a galactic fountain. The extent to which this affects the overall structure and distribution of the gas is unclear.

Agreement remains elusive when it comes to details such as the filling factor of the various phases, and poros-

ity of the medium (see reviews by Cox 2005; Ferrière 2001). These depend on the number and energy distribution of supernova events, and how they interact with the surrounding medium. The role of magnetic fields in the interaction is unclear, although some models of supernova evolution have incorporated their effects (e.g. Slavin & Cox 1992). In the Slavin & Cox (1993) picture, for example, the disrupting influence of supernovae is relatively small. However, the energy inputs of shells are imperfectly understood. The number and size of large shells in the outer galaxy cannot yet be explained by the expected level of star formation in those regions, despite consideration of numerous alternatives (see McClure-Griffiths et al. 2002).

Because H I shells are central to our understanding of the ISM, it is important to identify shells at all stages of evolution for further study. Early shell identification (Heiles 1979, 1984) was based on visual inspection of data, and so included non-expanding shells. Later searches for shells (McClure-Griffiths et al. 2002; Ehlerová & Palouš 2005; Daigle et al. 2007) commonly used expansion as one of the criteria for shell identification. This had the advantage of discriminating against random superpositions of filamentary gas, but the disadvantage of biasing the shell catalogs against older, more evolved shells. The most recent searches (Ehlerová & Palouš 2013; Suad et al. 2014) do include non-expanding structures, but are based on relatively low-resolution data. Previous searches carried out in high-resolution data are restricted to within a few degrees of the Galactic plane (McClure-Griffiths et al. 2002; Daigle et al. 2007).

In this paper, we present shells found in a visual-identification search of high-resolution data, in order to extend the Galactic census of H I shells. The SETHi

Electronic address: ssallmen@uwlax.edu

¹ University of Wisconsin - La Crosse, La Crosse, WI 54601² Space Sciences Laboratory, University of California at Berkeley, Berkeley, CA, 94720³ Milwaukee, WI⁴ Materials Science and Engineering Department, University of Maryland, College Park, MD 20742⁵ Hong Kong, China

(Search for Extraterrestrial H I) dataset is described in Section 2. We describe the search methodology and discuss the completeness of our search in Section 3. We present our search results in Section 4 and compare our findings to those of other surveys in Section 5. In Section 6 we discuss the physical properties of the shells and what our observations tell us about shells in our Galaxy.

2. DESCRIPTION OF SETHI SURVEY

When this work was performed, the SETHI survey was the single-dish large-scale survey with the highest angular resolution. Although interferometric surveys have higher resolution, the typical sensitivity of the SETHI survey exceeded that of the available interferometric surveys. SETHI also covered a larger range of Galactic latitudes than interferometric surveys, which are typically limited to within a few degrees of the Galactic plane. The Galactic Arecibo L-Band Feed Array H I (GALFA-H I; Peek et al. 2011) Survey was not available when this project began, and until its H I Data Release 2, expected in mid- to late-2016, still has less complete sky coverage than the SETHI survey.

SETHI was an outgrowth of the University of California, Berkeley (UCB) SETI program. Between 1999 and 2006 these searches used an uncooled receiver on the 1420-MHz flat-feed on Carriage House 1 at the National Astronomy and Ionospheric Center’s 305-meter radio telescope in Arecibo, Puerto Rico. This carriage house is opposite the zenith from the primary receivers in the Gregorian dome, allowing observations covering most of the Arecibo sky to be conducted while not interfering with other uses of the telescope. This resulted in two main modes of observation. When the primary feed was stationary or stowed the flat-feed beam scanned across the celestial sphere at the sidereal rate. If the primary observer’s feed was tracking a position on the celestial sphere, the Carriage House 1 beam scanned the sky at approximately twice the sidereal rate. At twice the sidereal rate, the 6′ half power beam width corresponds to a 12 second duration for a source to cross the beam. Over the duration of this survey, a large majority of the sky visible to the Arecibo telescope was covered. (Korpela et al. 2002, 2004).

The time domain data for the sky survey were recorded as follows: first, a 30-MHz band from the receiver was converted to baseband using a pair of mixers and low-pass filters. The resulting complex signal was digitized, then filtered to 2.5MHz using a pair of 192 tap FIR filters in the SERENDIP IV instrument (Werthimer et al. 1997). Single bit samples (one real and one imaginary bit per complex sample) were recorded on 35-GB DLT tapes. These were shipped to Berkeley for the SETI@home program.

The SETHI survey analyzed these tapes to extract hydrogen spectra. The 2.5-MHz time series data were converted to raw spectra using 2048 point FFTs ($\Delta\nu=1220$ Hz). We then accumulated 6144 spectra into a single power spectrum with an integration time of 5.033 seconds. The resulting power spectrum was corrected for one-bit sampling effects by applying the Van Vleck correction. The spectrum, its start and end coordinates, and the observation time were stored in a database.

Because no absolute power calibration was available in the receiver or recorder subsystem we calibrated our

Table 1
Comparison of the parameters of the LDS and SETHI surveys

Parameter	Leiden/Dwingeloo	SETHI
Angular Resolution (HPBW)	0.6°	0.1°
Spectral Resolution	1.0 km s ⁻¹	0.25 km s ⁻¹
Spectral Range	1000 km s ⁻¹	520 km s ⁻¹
Sensitivity	0.07 K	0.25 K
Sky Coverage	$\delta > -30^\circ$	$7.2^\circ < \delta < 29.7^\circ$

observations using existing surveys. We first performed a polynomial fit to remove broadband background variations, then implemented a system temperature calibration by performing a linear fit of the SETHI spectra to spectra from the Leiden-Dwingeloo survey (LDS; Hartmann & Burton 1997). While this method has the drawback of reducing our sensitivity to changes in **total** H I column density on scales smaller than the LDS beam size (36′), changes in the spectral velocity profile are well preserved on scales near the SETHI beam size. The more effective calibration developed for the GALFA-H I Survey (Peek et al. 2011), requires some observing techniques that are inapplicable to SETHI.

The spectral fitting resulted in an estimate of the system temperature (including any background continuum components). Our system temperatures fell between 60 and 170 K approximately 65% of the time. Excursions outside of this range due to receiver problems or excessive noise environments resulted in unusable data which we excluded from further processing.

The SETHI data were accumulated into 256×256×1591-pixel data cubes (RA, Dec, V_{LSR}) of dimension 7.68°×7.68°×410 km s⁻¹. Pixel dimensions in these cubes are 0.03°×0.03°×0.26 km s⁻¹.

Table 1 shows a comparison of the parameters of the LDS and SETHI surveys. The Leiden/Argentine/Bonn H I (LAB; Kalberla et al. 2005) survey’s sensitivity and resolution (both angular and spectral) are not significantly different from those of the LDS. While having superior spatial and spectral resolution, the SETHI survey’s spectral range, sensitivity and sky coverage are inferior to the LAB/LDS survey. If both surveys were at the LAB/LDS angular and velocity resolution scales, SETHI’s sensitivity is potentially 33 times better than quoted. The SETHI survey is prone to artifacts matching the grid spacing of the LDS spectra, because of the limits of single-bit data and the cross-survey calibration mechanism. Nonetheless it is useful for finding faint features on scales smaller than the LAB/LDS survey resolution.

3. METHOD

Because the SETHI survey covers a constant-declination strip of the sky, we performed our search in equatorial coordinates. For the purposes of this study, we merged the standard SETHI cubes into larger overlapping cubes. Each was 22.5° on a side, with a pixel size of 0.03° and a velocity resolution of 1.55 km s⁻¹. These cover the full range of RA, and are centered at a declination of 18.5°. The velocity range was restricted to exclude distinctly extragalactic gas, extending from -119.02 km s⁻¹ to 289.35 km s⁻¹.

3.1. Why Visual Identification?

With the increased velocity and angular resolution of current surveys, searching by eye is a daunting task. Nonetheless, purely automated searches are extremely difficult, as they work best for closed, regular, expanding structures. For example, the method of Mashchenko & St-Louis (2002) and Mashchenko et al. (1999) is based on the results of hydrodynamic models, and is problematic due to the non-uniformity of the ISM (e.g. fragmented or non-spherical shells, variations in background or foreground emission).

At the start of our search process, the most complete automated search for shells to date was the catalog of Ehlerová & Palouš (2005) based on the LDS, which covered 79% of the sky at an angular resolution of 0.5° . The catalog contained only closed structures with signs of expansion based on their central spectra, and selected against low-contrast shells in a rapidly changing background. Its completeness was best for younger shells (smaller, not blown out, not very distorted), but it was very incomplete for fragmented older shells with minimal expansion. For such large, irregular, non-expanding and possibly open structures, visual identification was the preferred technique (Ehlerová & Palouš 2005). This search was recently updated to eliminate the requirement that shells show evidence of expansion, and extended to the whole sky using the LAB survey (Ehlerová & Palouš 2013). Their algorithm still requires closed structures, meaning fragmented older shells are likely to be missed.

The higher angular resolution of the SETHi data means the incomplete nature of shell walls is more evident, making a visual search very appropriate. In addition, automated searches are much more computationally intensive for high-resolution data, and are frequently limited to younger expanding shells. The completely automated search of Daigle et al. (2007) used neural networks to identify small expanding shells in high-resolution data of a small ($48^\circ \times 9^\circ$) section of sky. Although non-uniformity of the ISM and possible extreme variations in shell shape make visual identification of shells subjective, the same issues also make it difficult to specify appropriate criteria for automatic searches (Daigle et al. 2007). Recently Suad et al. (2014) utilized a visual search to train an automated search algorithm focusing on super-shells in lower-resolution data, acknowledging that “the eye is an incredibly powerful instrument, especially when images are irregular”.

Due to the complex structures visible in our high-resolution data, and since every search technique requires visual inspection at some stage, we chose to take advantage of the human visual system. The procedure we followed does not require that the shell be expanding, although shells are deemed to be of higher “quality” if signs of expansion are present. Similarly, it allows for the identification of partial or fragmented shells. Care must be taken, however, to maximize consistency in shell identification and classification.

3.2. Description of Search Process & Criteria

The merged SETHi data cubes were viewed using the <kvis> program of the Karma Toolkit (Gooch 1996). To minimize errors and missed features, a minimum of two undergraduate students searched each cube using scal-

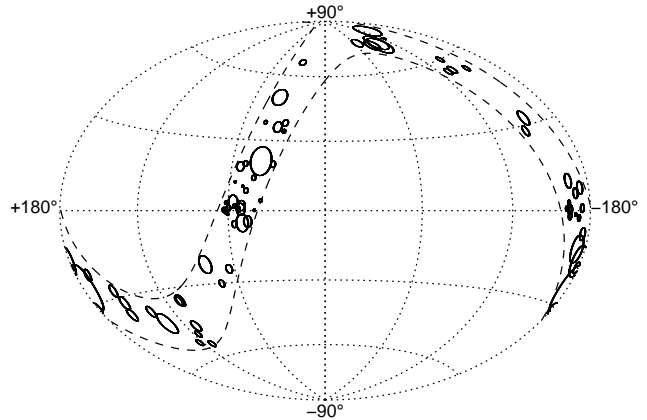


Figure 1. Sky plot of 74 shells newly identified in the SETHi dataset, in Galactic coordinates. The dashed line shows the limits of the SETHi data. Circles reflecting shell locations and mean angular diameters in equatorial coordinates were projected onto this representation.

ings chosen to highlight features in regions of both strong and weak emission. This resulted in a tentative list of 80 shells, 28 of which we eliminated as previously cataloged (Ehlerová & Palouš 2005; Ehlerová et al. 2001; Heiles 1984; Hu 1981; Heiles 1979). Fifteen (15) additional features were removed after further inspection by Korpela and Sallmen. We then searched all data cubes for missed shells, adding 28 convincing unknown shells to our list. Data cubes including the Galactic plane were given extra attention. During our exploration our catalog’s completeness (Section 3.3), we found 9 additional shells and added them to our catalog.

For all 74 shells in our final catalog we identified the velocity at which the shell is most evident (V_{ref}) and estimated the position of its center (RA, Dec), angular extent (ΔRA , ΔDec), and the range of velocities over which it appears “shell-like” (V_1 and V_2). Typical errors in central and edge position estimates are about 0.25° for small shells (less than 5° across), 0.5° for large shells (5 to 10° across), and up to 1° for very large shells (greater than 10° across). For a few shells with one edge near the declination limits of our data, we used the LDS data to estimate ΔDec . Note that V_{ref} may not be the central velocity of an expanding shell, but was defined to be valid even for old, non-expanding shells.

To determine mean angular diameters ($\Delta\theta$) for each shell, we identified the four locations at the ends of the long and short axes, then averaged the axis length estimates ($\Delta\theta_1$ and $\Delta\theta_2$). We define a shape parameter $S = 1 - (\Delta\theta_1 - \Delta\theta_2)/2\Delta\theta$ to describe the elongation of the shell. Note that $S = 0$ for a line, and $S = 1$ for a perfect circle. However irregular shells often lack well-defined short and long axes, making these measurements subjective on shells of that type, particularly for triangular or complex shapes. To quantify likely uncertainties, $\Delta\theta$ and S estimates made by multiple (two to five) people were compared for nearly all shells. Approximately 80% have differences in mean angular diameter of $< 10\%$; the same was true of the shape parameter for $\sim 85\%$ of shells. Reasonable differences of opinion larger than this (but $\lesssim 20\%$) occur mostly for shells that are relatively small, have very thick or irregular walls, or more than one of these characteristics.

Figure 1 shows the locations and sizes of these 74 shells on an Aitoff projection of Galactic coordinates. For each shell, we projected a circle with diameter equal to its mean angular diameter $\Delta\theta$ in equatorial coordinates. Our search identified a number of relatively small shells at a wide range of Galactic latitudes, due to the unique characteristics of the SETHI survey. Near the Galactic plane, many new small shells were identified, but few large ones remained unknown in this well-studied part of our Galaxy.

To determine the “quality” of each shell, we estimated the following quantities.

1. The fraction (f_{closed}) of the shell which is “closed” at V_{ref} , taking into account the weight/strength of the walls. $f_{\text{closed}} = 1$ for a shell which is 100% clearly and evenly closed.
2. The shape parameter S defined above. More regular shells are more believable.
3. The consistency (C) of the feature’s shape and location across the range of velocities (ignoring size changes). $C = 1$ implies both consistent shape and location. High scores indicate persistence in velocity, making the structure less likely to be a random overlay of disconnected features.
4. Fraction (f_v) of the velocity range over which the shell completeness remains at the value f_{closed} . Higher values result in more convincing shells. If one wall is visible at velocities where the others are not, the shell might be strongly sheared, or the structure might not be a shell.
5. Whether the shell appeared smaller in maps towards the velocity extremes, and largest near the central velocity. Half of the consistency score (C_θ) was allotted to each end of the velocity range. $C_\theta = 1$ is a clear signature of an expanding shell, while $C_\theta = 0$ if the shell size remains unchanged (or does not do what is expected). Intermediate values were based on a qualitative perception of how convincing the size changes were.
6. Whether any sign of expanding front and rear walls of the shell were visible in the maps at higher and lower velocities. Half of the wall detection (W) score was allotted to each cap. $W = 1$ indicates clear and unambiguous identification of both front (approaching) and rear (receding) walls, while $W = 0$ indicates no evidence of either wall, and no possibility of confusion limiting our detection ability. Intermediate values were based on qualitative perceptions of confusion levels and wall identifications.
7. Did we observe any sign of expansion in position-velocity (PV) space, i.e. in the Vel-RA and Dec-Vel maps? For each of these, we assigned a score from 0 to 1 based on the credibility of velocity splitting, and its consistency with previously determined size indicators. (PV : 0.3 for any splitting, 0.5 for matching range in position and velocity, 0.2 for maximum velocity in shell center). Scores for

the Vel-RA and Dec-Vel indicators were averaged to produce the final value.

We combined the first four parameters (f_{closed} , S , C , and f_v) into an overall quality estimate (Q), and the last three parameters (C_θ , W , and PV) into an expansion quality estimate (Q_{exp}), as the former do not depend on shell expansion. To facilitate their comparison, both Q and Q_{exp} were scaled to a maximum value of 10. Scatter plots and correlation estimates of each parameter against both quality scores confirmed that this division was appropriate. Other measured quantities (such as mean angular diameter or the velocity range over which the shell appeared shell-like) did not correlate with either quality score. These quality estimates do not necessarily reflect how convincing a shell looks at its reference velocity, because low scores for its shape and/or wall strength at the reference velocity may be offset by high scores in other contributing factors.

After completing the catalog and much of the analysis below, new H I shell lists were published by Ehlerová & Palouš (2013) and Suad et al. (2014). We have examined the overlap between our new list and these lists, but did not remove any additional shells from our catalog. We discuss specific cases of commonality in Section 4.1 and the overall comparison in Section 5.

3.3. Exploring Catalog Completeness

The process of visual search and identification is necessarily subjective, as H I sensitivity is not even across the survey, and shell detection depends on image display settings and individual perceptions. Although we made a point of having at least two individuals search each data cube at a variety of scalings, interstellar features could have been missed. The completeness of our search was explored by choosing four data cubes and re-examining them thoroughly. Two of these cubes included the Galactic plane, while the others were at high Galactic latitudes. For each, Korpela & Sallmen strived to identify all potentially shell-like features, and evaluated whether we would include them in the catalog using the categories Yes, No, and Possibly. We then compared this feature list with existing shell catalogs, as well as new SETHI shells identified during our original search.

During this second-look process we identified 32 features as worthy of catalog inclusion. Of these, 11 were already in our catalog, and 12 others had previously been published. However, we added 9 new shells to our catalog; 6 in the Galactic plane and 3 at high latitude. Similar extra attention to the remainder of the SETHI data would likely result in additional entries, but the number is difficult to quantify. We also identified 33 features as possibly worthy of inclusion, 22 of which we either failed to identify or rejected during our initial search. These results illustrate the subjective nature of our criteria for catalog inclusion of borderline shell-like features, but we did not add these to the catalog.

Prior to this second look, we had previously cataloged 31 shells with centers in these four SETHI cubes. However 3 were near the cube edges, so more easily recognized in adjacent overlapping data cubes. During our second-look process, we re-identified 22 of the remaining 28 shells, and categorized 19 of them as Yes or Possibly worthy of catalog inclusion. Some of the remaining cata-

log shells are complex features that overlapped or merged with other interstellar features when stepping through the velocity slices. For others we noted poor contrast or wall definition, suggesting they were on the borderline in our previous evaluations. Nonetheless, some shells are missed each time a cube is searched, validating our use of multiple individuals searching the data.

The SETHi catalog is subject to several selection effects. Firstly, our shell detection rate depends on shell size. Shells bigger than 10° to 15° are difficult to identify in our 22.5° data cubes, especially if they cross cube boundaries. Although we explored overlapping data cubes to mitigate this issue, shells extending beyond the data's Declination limits are not detectable. This especially limits the detection of large shells. Despite the data resolution, shells smaller than about 3° become more difficult to identify due to the large size of the search region. For such small shells, only those with sharp edges and high contrast are likely to be spotted. This effect makes shells smaller than about 1° very difficult to detect through our search method.

Our sensitivity to interstellar features also varies slightly across the dataset, partly due to the involvement of multiple students and the long time frame of the search, but also due to variations in the appearance of Galactic gas in different directions in the regions available to the Arecibo telescope. Because we expect shells to be more numerous in the Galactic plane, we ensured that data covering those regions received extra attention. These shells are extremely useful as potential targets for future study because they have low Galactic latitudes, so are more amenable to kinematic distance estimation. Despite the additional consideration, the completeness here may be somewhat less than other regions, due to the increased complexity of interstellar gas. Finally, the velocity range of the data does not fully cover Galactic gas; our data exclude some very distant spiral arms which may have different properties from more local ones.

4. RESULTS

Table 2 presents the SETHi shell catalog. Columns 1-4 contain the Shell identifier, equatorial coordinates (RA, Dec), and reference velocity at which it is most clearly identifiable (V_{ref}). Columns 5-8 describe the shell's spatial and velocity extent (ΔRA , ΔDec , V_1 , V_2). Columns 9-10 contain the mean angular diameter ($\Delta\theta$) and shape parameter (S). Columns 11 and 12 contain numerical estimates of the overall shell quality (Q and Q_{exp}). Flags in column 13 point the reader to additional comments (see Section 4.1).

All search results in Tables 2 through 6 are available at http://setiathome.ssl.berkeley.edu/~shauna/SETHi_Shells.html, along with links to images and summary information for each shell. The information provided assists the SETHi data and catalog user in identifying shells within the equatorial-coordinate maps. The SETHi data cubes may also be retrieved here.

The HI maps for 6 shells selected from our catalog are shown in Figures 2 and 3. Each is described briefly below.

GSH 052+10-087 is the smallest shell in our catalog, with a mean angular diameter of $\Delta\theta = 1.0^\circ$. It is extremely round ($S = 0.95$), high in quality ($Q = 8.7$; $Q_{\text{exp}} = 6$), and lies in high-velocity gas ($V_{\text{ref}} = -87 \text{ km s}^{-1}$).

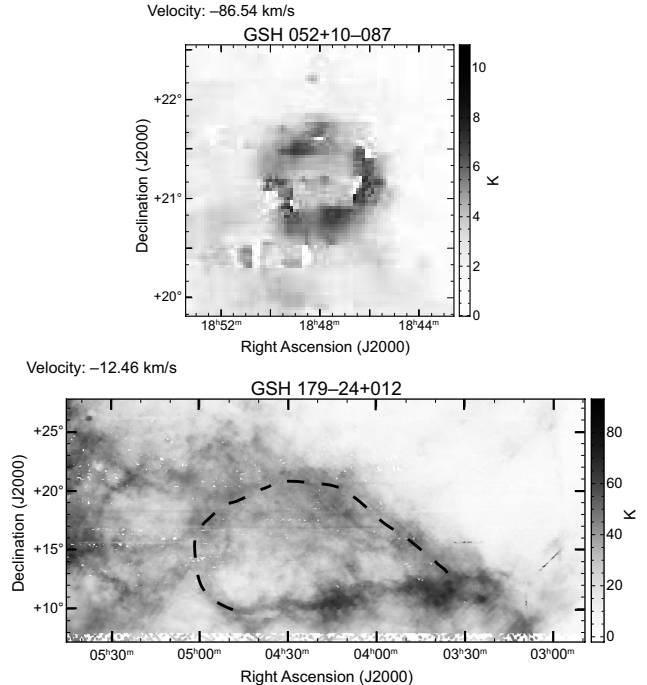


Figure 2. Neutral hydrogen maps for shells GSH 052+10-087 (top), and GSH 179-24+012 (bottom). Each shell is shown at its reference velocity. Darker shadings indicate regions of greater H I emission. The dashed line for GSH 179-24+012 indicates the extent of the shell in places where confusion might otherwise occur.

GSH 179-24+012 is the largest shell in our catalog ($\Delta\theta = 15.9^\circ$). Its teardrop shape ($S = 0.72$) extends from $01^{\text{h}}23^{\text{m}}$ to $05^{\text{h}}00^{\text{m}}$ in RA and from 9.75° to 21.5° in declination.

GSH 188+07-079 also lies in high-velocity gas, and has an irregular peanut shape. Its mean angular diameter ($\Delta\theta = 4.5^\circ$) is just above the average for our catalog. This moderate-quality ($Q = 4.6$; $Q_{\text{exp}} = 2.7$) shell is clearly non-spherical, giving it a low shape parameter ($S = 0.51$).

GSH 052-05+023 is an example of a shell that extends outward from the Galactic plane gas of a spiral arm. Based on our high-resolution data, we identified the extension at the northeast end as a separate shell (GSH 056-06+033). Both quality parameters are high ($Q = 7.5$, $Q_{\text{exp}} = 6.3$), as expected for a distinct part of a previously known expanding shell (see discussion in the next section). It is also one of the few shells for which we can estimate both kinematic distance and expansion velocity (see Sections 6.1.2 and 6.1.3).

GSH 052+02-071 is a low-contrast shell straddling the Galactic plane. Like many shells in our catalog, it shows little sign of expansion ($Q_{\text{exp}} = 1.8$), but has a high quality ($Q = 7.3$) based on its other characteristics.

GSH 225+55-005 ($\Delta\theta = 3.4^\circ$) is embedded in a region of complex gas. Because it is quite irregular in shape, its high shape parameter ($S = 0.92$) is misleading. It scores moderately well on visual parameters ($Q = 6.8$), but shows little evidence of expansion ($Q_{\text{exp}} = 0.8$). At $b = +55^\circ$, it lies well out of the Galactic plane, unless it is within local gas.

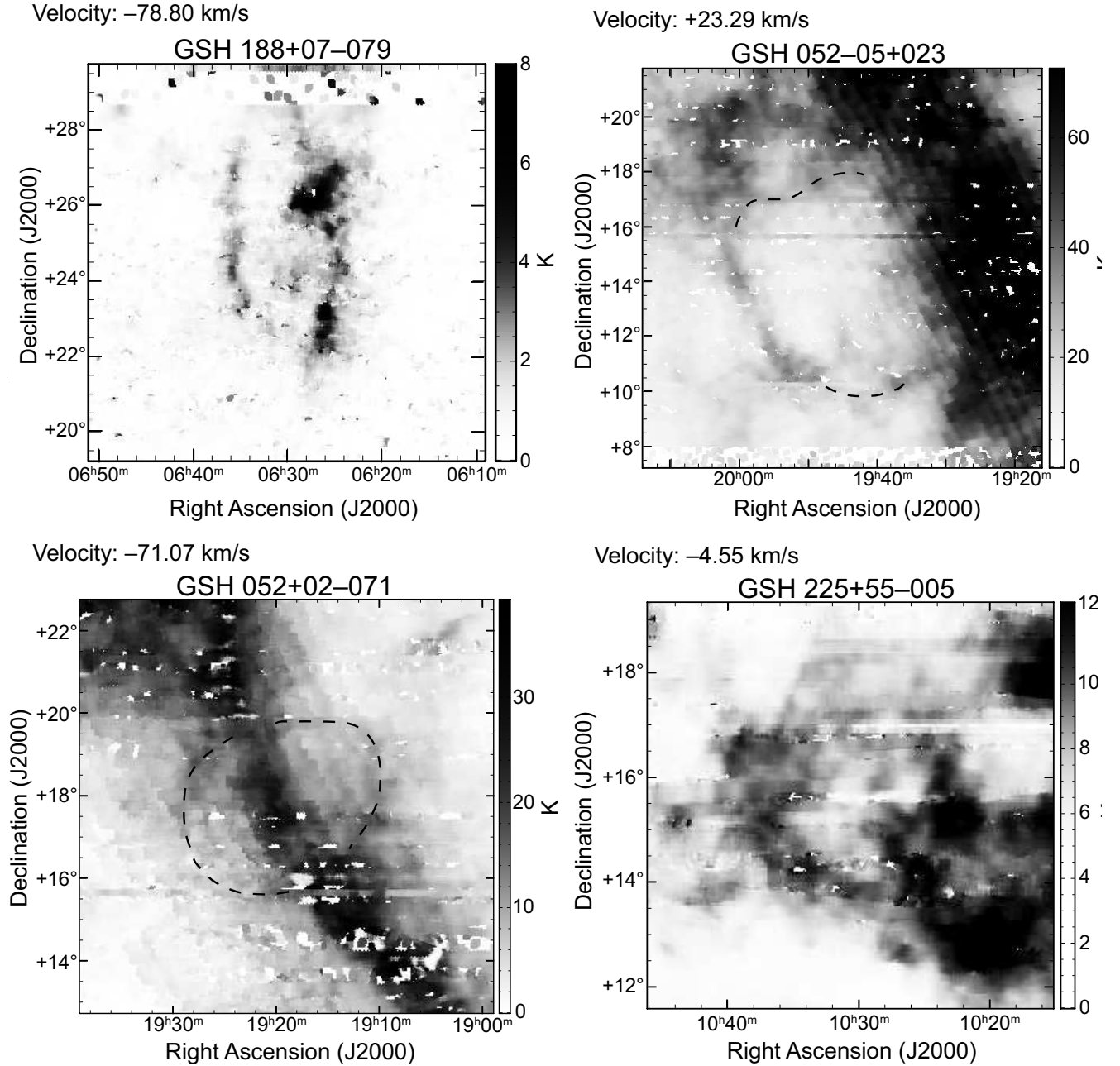


Figure 3. Neutral hydrogen maps for shells GSH 188+07-079 (top left), GSH 052-05+023 (top right), GSH 052+02-071 (bottom left), and GSH 225+55-005 (bottom right). Same as previous figure.

4.1. Comments on Shells in Table 2

For shells identified in Table 2's Comment column, noteworthy aspects are described below. This includes cases where our data conflicted with published shell identifications.

- **GSH 042+21+019** is a large structure related to the previously identified GSH 043+22+019, however Ehlerová & Palouš (2005) underestimated the extent of the shell. It is also not clear that their smaller GSH 037+19+016 is a separate entity.
- Based on how it appears across its velocity range,

GSH 048-05+045 is a large structure that contains GSH 047-03+040 (Ehlerová & Palouš 2005, small elongated feature at the southwest corner of our shell), as well as Heiles Supershell GSH 048-04+049 (Heiles 1979, east portion of our shell). At lower velocities, **GSH 048-05+045** blows out into a larger (unseen) bubble.

- Lots of confusion and data artifacts are present in the vicinity of **GSH 049+08+026**. Rather than being a shell, the feature might be composed of overlapping clouds.

- **GSH 052-05+023** and **GSH 056-06+033** may be related to one another, and both may be part of GSH 049-05+020 (Ehlerová & Palouš 2005) / GSH 050.0-05.0+019.6 (Ehlerová & Palouš 2013), which may be Heiles shell GS052-05+25 (Heiles 1979). However our high-resolution data suggest that these are two distinct features.
- **GSH 056+02-074** may be one piece of a larger shell. There might be a smaller adjacent shell or an additional piece of the same shell at similar velocities to the northeast, but we could not determine definitively due to localized data quality issues.
- Ehlerová & Palouš (2005) identified a feature inside of **GSH 057+04+005** as their GSH 057+03+003. Our larger shell is round, but of low contrast so difficult to discern.
- Based on our data, **GSH 062+00+045** contains GSH 061.5-00.5+046.4 (Ehlerová & Palouš 2013), and also additional regions to the northwest.
- The previously identified [EPH2001]62.1+0.2-18 appears to be part of our larger shell **GSH 063+00-022**. The field of view of Ehlerová et al. (2001) was only $4^\circ \times 4^\circ$, and cut off about half of this shell.
- **GSH 064-24+011** is the rightmost of two H I holes at similar velocities, possibly with break-through between them. Ehlerová & Palouš (2005) identified the combined features as a single shell, although the other half isn't very closed or shell-like. Our feature is GSH 064.0-24.5+011.3 in Ehlerová & Palouš (2013).
- For **GSH 134-43-062**, we chose $V_{\text{ref}} = -61.79 \text{ km s}^{-1}$ to maximize the feature's contrast. The north-south extent of the shell was estimated at -50.96 km s^{-1} , where the contrast is much lower but its upper and lower boundaries are identifiable.
- **GSH 155-32+005** is GSH 154.5-32.5+006.2 (Ehlerová & Palouš 2013).
- **GSH 156-37-003** is the northwest portion of the feature GSH 160.0-38.0-002.1 identified by Ehlerová & Palouš (2013). A substantial H I wall across their feature delineates the southern edge of our shell.
- **GSH 157-27-045** contains GSH 158-27-039 of Suad et al. (2014), as it is larger and more elongated than that structure.
- **GSH 180-31+020** is a relatively round shell with a dense diagonal stripe crossing it at the reference velocity.
- **GSH 192+06-017** was first reported in Korpela et al. (2004) and subsequently detected by Ehlerová & Palouš (2013).
- Although we chose to catalog them separately, **GSH 197-02+034** and **GSH 198+01+034** might be related to one another.

- **GSH 261+74-025** shares boundaries with the shell GSH 255+74-028 identified by Ehlerová & Palouš (2005), but our data clearly show a larger shell.

During our search we removed from further consideration shells previously discovered by others. As noted above, we retained features when our data were clearly in conflict with previous shell boundaries. In a few cases, we found the divisions to be subjective so did not include the shells in our catalog, but describe the possible differences below.

- GSH 248+69-013 and GSH 250+68-005 were previously cataloged separately by Ehlerová & Palouš (2005), while our impression is that this is a single low-quality shell that morphs somewhat in shape, location and size at various velocities.
- GSH 046+09+010 (Ehlerová & Palouš 2005) has two distinct lobes which may or may not be related. We would have considered cataloguing this as a single shell.

5. COMPARISON WITH OTHER SURVEYS

Since features identified as previously known shells were not always recorded by students during the initial search, we used the results of our second-look process (described in Section 3.3) to investigate how often we detected shells listed in catalogs published prior to spring 2013. Of the 62 known shells with centers in these four regions, we identified 17 during this examination of the data. Approximately half of the other 45 were either too big to be easily visible in our 22.5° cubes, or went off the edges of the cube. We examined our data for the remainder (~ 20), and attribute their non-identifications to one or more of the following reasons: (1) Poor contrast in our high-resolution data, particularly for shells from Ehlerová & Palouš (2005), as that search used ΔT while the SETHi search utilized $\Delta T/T$. (2) Poor shell closure and poorly defined walls in our higher-resolution data, when compared with their appearance in the lower-resolution data. (3) Shells were located in complex regions of high confusion, or in regions where the SETHi survey had poor data quality. (4) We rejected the feature because their shape and/or size changed substantially with velocity, or they showed poor persistence with velocity. For one or two shells, these factors were so extreme we couldn't identify the published feature in our data at all. Given the differences in our dataset and search criteria compared with previous work, these results are not surprising.

After our catalog and the above analysis was complete, two additional shell catalogs became available: Ehlerová & Palouš (2013) and Suad et al. (2014). We subsequently investigated potential overlap between these and our SETHi catalog. Of the 74 shells in our catalog, only three were also identified by one of these other searches. Three additional SETHi shells are clearly sub-sections of larger features in the other catalogs, and in two cases the other searches identified features clearly contained within a larger SETHi catalog entry. For all of these, the SETHi data reveal clearer shell boundaries for our classification choices. Finally, five more SETHi shells may be related

to entries in the other catalogs, although the connection is not clear given the SETHi data.

Our catalog comparison findings echo those reported by Ehlerová & Palouš (2013) and Suad et al. (2014): altering the search method and/or selection criteria strongly affects shell identification. They found this true even for searches using data of similar angular resolution; our catalog is based on data of much higher resolution, so substantially different results are to be expected. Our search is unique in exploiting the SETHi survey’s high angular resolution over a large range of Galactic latitudes.

We also explored the robustness of our shell identifications in higher-resolution data using the VLA Galactic Plane Survey (VGPS; Stil et al. 2006), which has lower sensitivity than the SETHi survey. Seven of our catalog shells are small enough ($\Delta\theta < 3^\circ$) and located within the VGPS data ($l < 65^\circ$; $|b| < 2^\circ$). For four of these, the VGPS data are consistent with our analysis, but reveal more detailed shell structure. Two are visible but not as obvious in the VGPS data, because the higher resolution accentuates wall fragmentation and the presence of faint wispy material within the shell. In one case (GSH 054+01+031), the high-resolution VGPS data suggest a very faint, thin wall at $b < 0$ that is not obvious in our SETHi data. The feature we identified as the low- b wall may be a cloud inside the shell. To maintain consistency in our catalog, we have not revised our measurements of this shell.

6. DISCUSSION

6.1. Physical Properties of Shells

6.1.1. Statistics of Shell Properties

Figure 4 shows the distribution of Quality Estimates Q (solid) and Q_{exp} (dotted) for the 74 shells in our catalog. Most shells have relatively high overall quality estimates Q , reflecting the fact that we did not measure shells we found less convincing. Our catalog is therefore less complete at the lower end of the range of Q values. However, most shells have low expansion quality estimates, validating that our approach avoids a significant bias against older slowly expanding shells.

Figures 5 and 6 display the distribution of mean angular diameters ($\Delta\theta$) and shape parameters (S) for our catalog. The average mean angular diameter is 4.1° , with a median value of 3.3° . Although the distribution extends to fairly large shells, most newly discovered shells are relatively small. Most larger shells were discovered in previous lower-resolution surveys. The lack of shells smaller than 1° is due to limitations in our survey resolution, calibration, and search methodology.

The shape parameters range from 0.44 to 0.99. The average S is 0.78, while the median is 0.79. Recall that $S = 0$ for a thin line and $S = 1$ for a completely round shell, although non-oval shapes can make this parameter misleading. Our catalog contains many shells with high shape parameters, possibly reflecting the fact that round features are more likely to be visually identified as potential shells. Extremely elongated features (which would have low S) were deemed poor shell candidates, so are not in our catalog.

Distributions of other measured quantities (not shown) were also examined. The shell wall completeness (f_{closed})

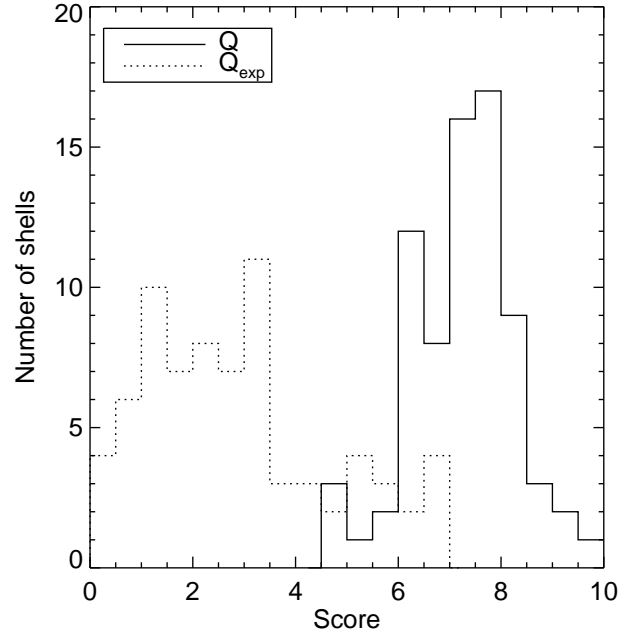


Figure 4. Distribution of Quality Estimates for the 74 shells in our catalog. The solid line shows the histogram of overall quality estimates Q , which are independent of evidence for shell expansion, while the dotted line shows the histogram of expansion quality estimates Q_{exp} .

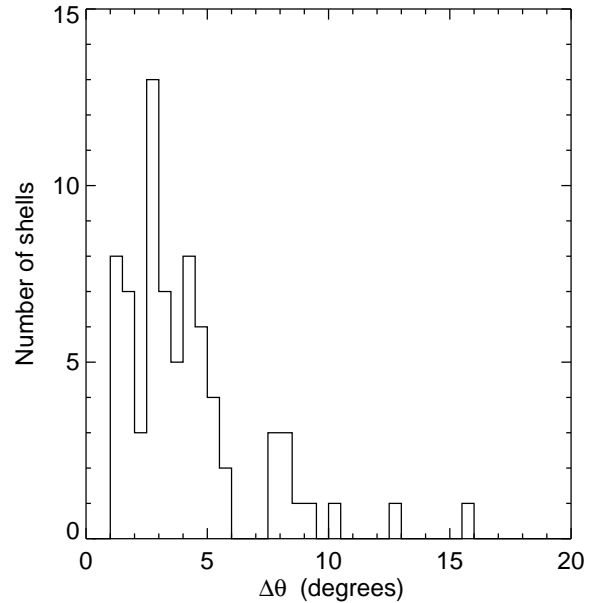


Figure 5. Distribution of Mean Angular Diameters ($\Delta\theta$) for the 74 shells in our catalog.

is always above 0.5, with a median value of 0.8, reflecting a visual-search bias towards regular shell walls. The distribution of morphological consistency with velocity (C) extends to values as low as 0.1, but the median is relatively high (0.7). Without strong additional indicators, structures with low C values were likely to be deemed overlapping gas features, rather than shells. On average, shells in our catalog were maximally closed over about 60% of their velocity range, with a standard deviation

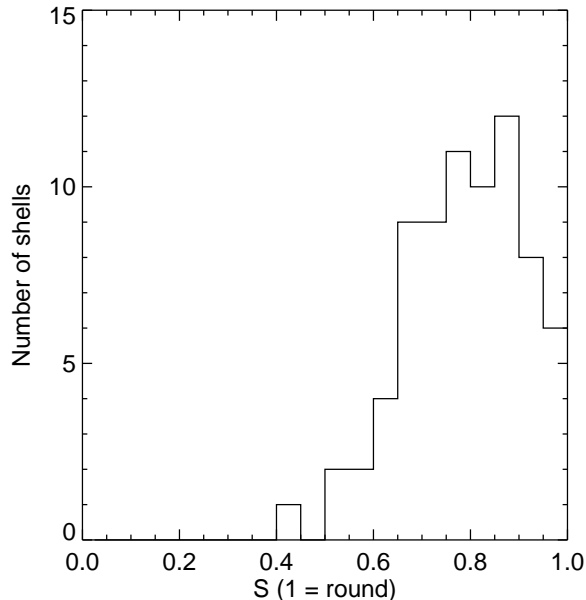


Figure 6. Distribution of Shape Parameters (S) for the 74 shells in our catalog.

of 17%. The distributions of expansion-related parameters (C_θ , W , and PV) all skewed towards lower values, approximately mirroring the Q_{exp} distribution.

We explored the possibility of correlation between mean angular diameter $\Delta\theta$ and shape parameter S , as well as whether either were correlated with Galactic latitude. None were observed, with linear correlation coefficient $r < 0.25$ in all cases.

6.1.2. Distances and Physical Sizes

For those shells with $|b| < 15^\circ$, we estimated a kinematic distance based on V_{ref} and the Galactic rotation curve of Brand & Blitz (1993). Velocities of some shells are inconsistent with Galactic rotation, so no kinematic distance determination was possible. In the inner galaxy there are two potential solutions, so two distances were determined where feasible. A range of possible distances (D_{min} to D_{max}) was estimated for each, using $|V_2 - V_1|$ and assuming the shell was centered on V_{ref} . Although V_{ref} is not always the center of the shell’s range of visibility, it is adequate in light of the uncertain nature of kinematic distances.

Peculiar motions complicate kinematic distance determination. Possible errors due to non-circular gas motions are not incorporated in the quoted distance ranges. Brand & Blitz (1993) estimate one-dimensional streaming motions in the Galaxy at $\sim 12 \text{ km s}^{-1}$, which adds substantial uncertainty in the derived distances. For example, Xu et al. (2006) estimated the peculiar motion of star-forming region W3OH at 22 km s^{-1} . This caused the kinematic and parallax distances to differ by about a factor of two (4 kpc vs. 2 kpc).

Of the 33 shells with $b < 15^\circ$, kinematic distances were derived for 27. Towards the anti-center ($l \sim 165^\circ$ to 195°), irregular gas motions may dominate the radial velocity effects of Galactic rotation, so results are less reliable. In Table 3, columns 1-3 contain the Shell identifier and its Galactic coordinates, while columns 4-6 contain

the kinematic distance D_{ref} corresponding to V_{ref} and the range of allowed distances (D_{min} to D_{max}). Columns 10-12 contain the second set of estimates for shells in the inner galaxy. Columns 7-9 and 13-15 contain size (diameter) estimates (S_{ref} , S_{min} , and S_{max}) determined from the corresponding kinematic distances and the shell’s mean angular diameter. Dashes (-) in columns 2-15 indicate no solution was found for that value. Column 16 contains a key to comments; most discuss the likelihood of kinematic distance options based on Galactic spiral structure and/or inferred shell sizes. Unless otherwise specified, shells are clearly associated with Galactic plane gas, so kinematic distances are relatively reliable. For convenience during later discussion, values for shells with single or preferred distance estimates are boldfaced in the table.

6.1.3. Shell Expansion

Knowing a shell’s expansion velocity is key for understanding its evolutionary state. We therefore derived spectra for all 18 shells showing moderate signs of expansion ($Q_{\text{exp}} \geq 4$). We defined both a spectral extraction region centered on the shell and a constant- b background extraction region at b_{shell} outside the shell boundary. The spectral extraction region’s size was scaled to a fraction of the shell’s mean angular diameter ($\Delta\theta$), as were the background region’s thickness, minimum distance and maximum distance from the shell center. At every velocity, raw and background spectral values were determined by averaging within each region. We then analyzed the normalized (raw – background) spectrum, identifying the local minimum nearest V_{ref} and the local maxima on either side, to estimate the velocities of the shell’s approaching and receding walls. For noisy spectra, we disregarded spurious local maxima and estimated the velocity of the appropriate peak(s). For each shell, this procedure was performed for three different choices of spectral and background extraction regions.

We examined the results in detail for every shell. This included careful evaluation of the appropriateness of the background region, especially where the shell is elongated towards it. Slight alterations were implemented if necessary to obtain a physically plausible scenario. In a few cases we repeated the analysis after slightly adjusting the location of the spectral extraction region, based on the shell’s shape and location variations with velocity. To evaluate their reasonableness and consistency, spectral analysis results were compared against one another, and against the shell region’s visual appearance at each velocity using $\langle \text{kvis} \rangle$. This often revealed that gas producing a spectral maximum was not unambiguously associated with the shell, and sometimes that it was clearly unassociated. In some cases, other adjacent spectral maxima were clearly identified as the shell wall. In addition, complex features of varying density in the background region obviously introduced spurious features in the normalized spectra of certain shells. If possible we adjusted the background region to minimize these effects, but often no alternative was available. In those cases we based our analysis on the local minima and maxima of the raw spectra.

For 7 shells, we identified both front and rear shell walls, and calculated $V_{\text{exp}} = (V_b - V_f)/2$. For a few, the identification of these features is relatively unambiguous.

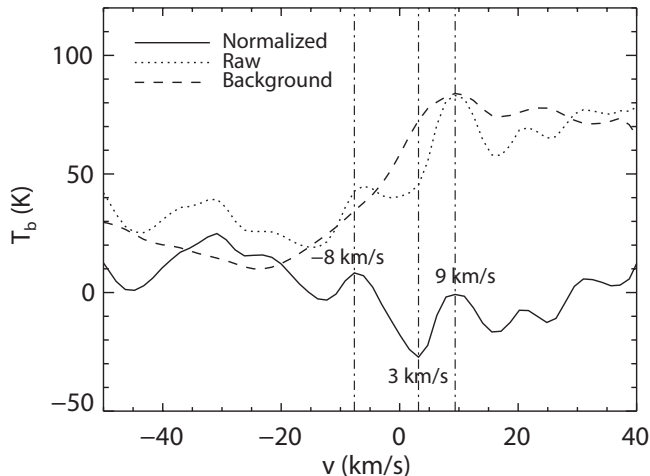


Figure 7. Raw (dotted) and background-normalized (solid) H I spectra through the center of GSH 054-00+003. The background (dashed) spectrum is from a constant- b region outside the shell, and was used to normalize the raw spectrum. The dash-dotted vertical lines mark the velocities of the front and rear walls, as well as the minimum H I intensity.

The spectra and identified minima/maxima are displayed in Figure 7 for GSH 054-00+003, whose expansion velocity ($V_{\text{exp}} = 9 \text{ km s}^{-1}$) is most certain. For the rest, unrelated clumps of gas might be confusing the spectrum, resulting in inaccurate estimates. For these we also present a lower limit on the expansion velocity based on the best wall identification and the furthest edge of the velocity range at which the structure appeared “shell-like” ($V_{\text{exp}} > (V_b - V_1)/2$ or $V_{\text{exp}} > (V_2 - V_f)/2$). For 5 other shells we were able to identify only the front wall or the rear wall, so could merely derive a lower limit to the expansion velocity. Inability to identify a front or rear wall for a shell is not unexpected, both because limb brightening makes them weak relative to the visible walls, and because high radial velocity dispersion in shell walls would produce a broad, weak spectral feature.

For 6 of the 18 shells we could not significantly constrain the shell expansion velocity: GSH 048-05+045, GSH 060+01-076, GSH 110-35-034, GSH 113-54-005, GSH 180-31+020, and GSH 208+32+006. In these, spectral features potentially denoting shell walls might be faint and uncertain, confused with other complex gas structures, in regions/velocities with poor data quality, or a combination of these factors. Due to the lack of limb-brightening at the shell center, sensitivity limitations might prevent us from identifying front or rear walls, even if the shell is expanding. In addition, if front or rear walls are incomplete or contain significant velocity dispersion, their spectral signature will be difficult to identify.

Table 4 displays the results. The first two columns contain the Shell ID and expansion quality parameter Q_{exp} . Columns 3-5 contain the velocities of the approaching front and receding back (rear) walls (V_f and V_b , respectively), and the resulting expansion velocity estimate. Columns 6-8 contain the shell-like velocity range V_1 & V_2 , and the lower limit on V_{exp} described above. The last column contains a key to comments regarding the process.

The quoted expansion velocities are often quite uncer-

tain. Given the velocity resolution of the spectra, the best-case scenario is an uncertainty in both V_f and V_b of $\sim 1.5 \text{ km s}^{-1}$, giving an uncertainty of at least $\sim 1 \text{ km s}^{-1}$ for V_{exp} . However, this is overly optimistic due to the image and spectral complexities described above. For GSH 054-00+003, we estimate an expansion velocity uncertainty of 1.5 km s^{-1} , with substantially larger errors for all other shells. We have greater confidence in the quoted lower limits; the actual expansion velocity is likely no more than $\sim 1 \text{ km s}^{-1}$ below these, although the possibility remains if we have mis-identified unrelated gas as part of the shell wall.

6.2. Other Derived Properties

Estimating the ages and energies of shells is important for understanding shell evolution and the changing ISM. Where we had shell physical size and expansion velocity information, we evaluated these quantities as follows. Note that we utilized only sizes derived from the actual kinematic distance estimates, and not the range of possible values.

For shells with estimates of both physical diameter S_{ref} and expansion velocity V_{exp} , we calculated an upper limit on shell age by assuming it has always expanded at its current rate, rather than slowing over time: $t_1 = S_{\text{ref}}/2V_{\text{exp}}$. Where two distance possibilities produced two estimates of shell size, a second age t_2 was also calculated. In cases where we only estimated a lower limit on V_{exp} , we used that to estimate the age upper limit(s).

For each shell with a physical size estimate, we used S_{ref} to estimate its current thermal energy, assuming shells are spherical, old and in rough pressure equilibrium with the ISM. For a shell of volume V , the approximate interstellar gas pressure $P_{\text{th}}/k \sim 3000 \text{ cm}^{-3} \text{ K}$ (Wolfire et al. 2003) gives a thermal energy of $E_{\text{th}} = (3/2)n k T V = (3/2)P_{\text{th}} V$. Where we had two size estimates, we calculated E_{th} for both. This energy estimate scales with the assumed pressure and is very uncertain, as the ISM is far from uniform. In addition, young shells with larger expansion velocities may not yet be in pressure equilibrium.

For shells with an expansion velocity (not just lower limits), we estimated the current kinetic energy as $E_K = 0.5 M_{\text{shell}} V_{\text{exp}}^2$. To evaluate the mass, we assumed the shell has been expanding into a constant-density ambient medium, and has swept up all the material in its spherical volume. We further assumed that the hydrogen density is $n = 1 \text{ atom cm}^{-3}$ and $n_{\text{He}}/n = 0.1$, but the results scale linearly with n , so can be easily altered for different density assumptions. This energy estimate is necessarily crude, given the non-spherical nature of most shells, the non-uniformity of the ISM, and the inherent uncertainty in shell sizes derived from kinematic distances.

For the same shells, we also calculated the initial total shell energy using Chevalier’s formula for a shell of radius r_{sh} now expanding with velocity V_{exp} into an ambient medium of hydrogen density n (Chevalier 1974), again assuming $n = 1 \text{ atom cm}^{-3}$.

$$E_{\text{Ch}} = 5.3 \times 10^{43} \left(\frac{n}{\text{cm}^{-3}} \right)^{1.12} \left(\frac{r_{\text{sh}}}{\text{pc}} \right)^{3.12} \left(\frac{V_{\text{exp}}}{\text{kms}^{-1}} \right)^{1.4} \text{ ergs}$$

Note that this formula is most reliable for smaller less

evolved shells, but can be an underestimate of the energy of larger shells, especially those with irregular shapes.

Table 5 displays derived physical properties of these shells, with Shell IDs in the first column. Columns 2 and 6 contain the age upper limits t_1 and t_2 corresponding to the two shell diameter estimates S_{ref} and $S_{\text{ref}2}$, respectively. Columns 3 and 7 display the two thermal energy estimates $E \times (P/3000 \text{ cm}^{-3}\text{K})$ corresponding to the two shell sizes, and columns 4 and 8 present the corresponding kinetic energy estimates $E_K \times (1 \text{ cm}^{-3}/n)$. The total energy estimate(s) $E_{\text{Ch}} \times (1 \text{ cm}^{-3}/n)$ are in columns 5 and 9. Column 10 contains codes indicating extra information, such as which values are more likely based on kinematic distance preferences described in Table 3, or how age upper limits were derived from expansion velocity (limit) estimates. For convenience during later discussion, the age and energy values are boldfaced for shells with single or preferred distance and size estimates.

6.3. Discussion of Shell Properties

For the majority of shells in Table 3, there is either only one distance solution, or other considerations such as Galactic spiral structure led us to prefer one solution. The exceptions are GSH 040+04+048, GSH 045+14+031, and GSH 049+08+026. We restrict the remaining discussion to the other 24 shells, for which the preferred distances suggest diameters ranging from 18 pc to 1500 pc, with the median at 440 pc, and the peak of the distribution at 250 pc. These shells are generally quite large, with only two having diameters < 200 pc, and only 7 smaller than 300 pc. Biases in our search procedure, and the elimination of previously known structures, limit the information present in this distribution. However these sizes are similar to those shown in Figure 6 of Ehlerová & Palouš (2005), and many of the larger sizes were judged plausible given the apparent shell size relative to the Galactic plane, as mentioned in the table notes. Shells this large must be caused by strong stellar winds and the supernovae of many stars. For comparison, the Loop I superbubble, likely generated by the stars of the Sco-Cen OB association, is ~ 200 pc in diameter (Nishikida 1999). Its expansion velocity of $\sim 20 \text{ km s}^{-1}$ suggests it is several million years old, although its X-ray intensity suggests an age of $\sim 10^5$ yr.

To evaluate whether the shells were preferentially elongated either perpendicular or parallel to the Galactic plane, we took the four locations used to estimate the long and short axes (as described in Section 3.2), converted them from equatorial to Galactic coordinates, then calculated the angle between the long axis and the Galactic plane. Table 6 contains the resulting semi-major axis (a), semi-minor axis (b), and position angle of the major axis ($\phi = \arctan(\Delta b/\Delta l \cos(b))$) in degrees for all 74 shells. The position angles span 0° to 180° , showing no preference for alignment parallel or perpendicular to the Galactic plane, and we see no evidence for variations in alignment with angular size $\Delta\theta$. This conflicts with previous work (Ehlerová & Palouš 2005; Ehlerová & Palouš 2013; Suad et al. 2014) that suggested most shells are elongated parallel to the plane. Since there is very little overlap between our catalog and those (and none with Ehlerová & Palouš (2005)), our search criteria and process may mean we are looking at a slightly different population of interstellar structures. We also suggest

that the trend in orientation found by others might result from a selection bias, as the low- $|b|$ edge of a structure could be truncated in visual or automated searches due to the increasing gas density towards the plane. Finally, many shells are highly irregular in shape, severely complicating orientation analyses based on $\Delta b/\Delta l \cos(b)$, elliptical fits, or visual identification of major & minor axes.

The expansion velocities and limits in Table 4 are all larger than 5 km s^{-1} , and mostly greater than 10 km s^{-1} . Recall, however, that expansion velocities were not determined for the majority of shells in the catalog, which show little or no signs of expansion. Those presented are therefore unlikely to be typical of the overall shell population. We also note that all expansion velocity measurements are less than 20 km s^{-1} , indicating these shells are relatively evolved. The corresponding ages presented in Table 5 are generally quite large, over 3.5 Myr in all but one case (GSH 054-00+003, but the larger distance and age is preferred). These are upper limits, however, and the actual age is likely less than about half of the values given.

To put shell energy estimates into context, a typical supernova initially has $\sim 10^{51}$ ergs of kinetic energy. However, heat, interstellar turbulence, and radiation have dissipated most of this energy for older, evolved shells. By the time a supernova remnant (SNR) has slowed to 10 km s^{-1} , the kinetic energy of a shell is reduced to less than about 10% of its initial value, and can be much lower if the density of the ambient medium is sufficiently high (e.g. Chevalier 1974; Spitzer 1978; Thornton et al. 1998). For an evolved single-supernova shell, we therefore expect current energy estimates of order $\sim 10^{50}$ ergs.

We have a total of 37 current thermal energy estimates for 27 shells, 24 of which have either only one energy estimate, or one that is preferred as noted in Table 3. Similarly, we have a total of 10 current kinetic energy estimates for 6 shells, 5 with single or preferential values. In what follows, we consider only these single or preferential energy estimates (bold-faced in Table 5). The median thermal energy estimate is 8.6×10^{50} ergs, while the median kinetic energy estimate is 1.0×10^{51} ergs. Nearly all these current shell energies are consistent with an evolved shell produced by at least one supernova, often more. The few shells with much lower thermal energy values may be a result of inaccurate kinematic distances, the crude nature of our energy estimates, and/or a different evolutionary history for the shell. For shells expanding into the Warm Ionized Medium (WIM), the ambient density could be as low as $n = 0.1$ for some shells, which would decrease the calculated kinetic energies by a factor of 10. For this density, the kinetic energies of GSH 054-00+003 and GSH 054+01+031 fall below 10^{50} ergs; however these shells appear embedded near Galactic plane gas, so the ambient density is likely higher than this minimum value.

In contrast to the thermal and kinetic energy estimates, E_{Ch} estimates the energy required to create each structure. We evaluated this total energy for 6 shells, 5 of which have single or preferential distances/sizes. For these 5, the median value of E_{Ch} is 1.3×10^{52} ergs, with all of the estimates greater than 10^{51} ergs. In general, this suggests that most shells required the energy input of

multiple supernovae for their formation, however all energy estimates assumed $n = 1$ hydrogen atom cm^{-3} . For the smallest likely ambient density in the WIM ($n = 0.1$), the calculated total energies would decrease to 8% of their tabulated values. In this case E_{Ch} for two shells would fall below 10^{51} ergs, to $\sim 3 \times 10^{50}$ ergs. However as noted earlier, both these shells lie in or near higher-density Galactic plane material. In addition, recall that E_{Ch} , based on single-supernova models, can be an underestimate for large shells such as these.

6.4. GSH 054-00+003

We now consider GSH 054-00+003 in more detail, in the context of SNR modeling. Recall from Tables 3, 4 and 5 that it has an expansion velocity of 9 km s^{-1} , a radius of 120 pc, a current kinetic energy $E_K = 2.1 \times 10^{50}$ ergs, and a total energy $E_{Ch} = 3.8 \times 10^{51}$ ergs, taking the preferred distance and assuming $n_H = 1 \text{ cm}^{-3}$. If the energy of a single SN is $E_{SN} = 10^{51}$ ergs, E_{Ch} suggests several supernovae together produced GSH 054-00+003. According to the models of Figures 8 and 9 of Thornton et al. (1998), a supernova expanding into material with this density will grow to $r_{sh} \sim 75$ pc by the time it has slowed to $V_{exp} \sim 10 \text{ km s}^{-1}$. At this time (~ 2 Myr) the SNR will have a kinetic energy $E_{K,mod} \sim 3.8 \times 10^{49}$ ergs (4% of its initial E_K). Thus ~ 6 supernovae would be required to produce the current kinetic energy of GSH 054-00+003, while a comparison of the observed and model shell volumes would suggest ~ 4 supernovae are required. These are consistent with the estimate based on E_{Ch} .

We chose a hydrogen density of $n = 1 \text{ cm}^3$ because this shell is clearly embedded in relatively dense Galactic plane gas near a spiral arm. In addition, Thornton et al.'s models suggest that for $n \sim 0.1 \text{ cm}^{-3}$ (appropriate for the Warm Ionized Medium), a single SNR would be $r_{sh} \sim 140$ pc by the time it has slowed to $V_{exp} \sim 20 \text{ km s}^{-1}$, thus becoming larger than the observations for GSH 054-00+003 before slowing to the observed expansion rate. Also, E_{Ch} for this case is less than 10^{51} ergs. But if the embedding gas has a density of $n = 10$, the models of Thornton et al. (1998) suggest a single-supernova SNR will have a radius of 30 pc and a kinetic energy of 2.5×10^{49} ergs when its expansion has slowed to the observed value (~ 0.6 Myr), in which case the observed volume and current kinetic energy (which scales as n) suggest ~ 60 -90 supernovae are required to form the shell. The estimated total shell energy E_{Ch} in this case is ~ 50 times the energy of a single supernova.

Finally, note that the large age estimates are more consistent with the absence of enhanced 0.25 keV X-ray emission (Snowden 1977) from the direction of GSH 054-00+003 (accessed using *SkyView*; McGlynn et al. (1998)).

7. CONCLUSIONS & FUTURE WORK

Our visual search of the SETHi database resulted in the identification of 74 previously unknown interstellar shells. The catalog is uniquely based on high-resolution data that is not limited to the Galactic plane, and is not biased against older non-expanding shells, unlike many earlier searches. It is also more sensitive to irregular shells with fragmented walls than most automated searches. We presented basic measurements (position, reference velocity, angular size, elongation, position angle) for all 74 shells, along with kinematic distances,

physical sizes, and expansion velocities where possible. Shells in the catalog with kinematic distances are large, old, and expanding relatively slowly if at all. Energy considerations suggest they all formed by multiple supernovae. In contrast to findings by others, our catalog shells are not preferentially elongated either parallel to or perpendicular to the Galactic plane.

The SETHi dataset has better angular resolution than the LAB/LDS used by most previous large-scale searches, and includes high Galactic latitudes, unlike other high-resolution H I surveys. The GALFA-H I Survey now provides higher-quality data with these characteristics, but was not available when this labor-intensive project began. The GALFA data are currently best at declinations complementary to those we examined here, so a future search based on GALFA data will add to the census of Galactic H I shells.

Galactic radial distribution, size distribution, and filling factor of H I shells are of interest for modeling the Galactic ISM. However, this catalog is incomplete on its own. Where there is spatial overlap, combining it with other large-scale catalogs would require careful consideration of the different nature of the underlying data. The identification biases and sensitivity limitations are also drastically different for the varied search techniques. In addition, size and shape measurements based on equatorial coordinates are difficult to directly compare with those of catalogs delimited in Galactic coordinates. To assist with this issue, we provided the estimates of semi-major/minor axes and position angles. If such an integration were to be carried out, it would also enhance data on the distribution of shell sizes and their number relative to distance from the Galactic plane, or Galactic longitude.

During this work Dr. Korpela was supported in part by NASA grant NNX09AN69G and NSF grant AST-0709347. Dr. Sallmen was supported in part by NSF grant AST-0507326, the Research Corporation (Cottrell College Science Award No. CC6476), and by NASA/Wisconsin Space Grant Consortium's Research Infrastructure Award Program.

The SETHi Survey was funded by the National Science Foundation through grant AST-0307956 with technical support provided by the staff of the Arecibo Observatory. The Arecibo Observatory is part of the National Astronomy and Ionosphere Center which was, during the course of this work, operated by Cornell University and Universities Space Research Association under Cooperative Agreements with the National Science Foundation.

Kevin Douglas produced the $7.68^\circ \times 7.68^\circ$ SETHi data cubes that were combined and utilized in this analysis. La Crosse undergraduate students Lillian Kasel, Tyler Laszczkowski, and high school student Daniel Morrison assisted with portions of the shell measurements.

We acknowledge the use of NASA's *SkyView* facility (<http://skyview.gsfc.nasa.gov>) located at NASA Goddard Space Flight Center. This research has made use of the SIMBAD database, operated at CDS, Strasbourg, France (Wenger et al. 2000).

Facilities: Arecibo.

REFERENCES

- Brand, J. & Blitz, L. 1993, *A&A*, 275, 67
 ADS:1993A&A...275...67B
- Chevalier, R. A. 1974, *ApJ*, 188, 501 doi:10.1086/152740
- Cox, D. P. 2005, *ARA&A*, 43, 337
 doi:10.1146/annurev.astro.43.072103.150615
- Daigle, A., Joncas, G., & Parizeau, M. 2007, *ApJ*, 661, 285
 doi:10.1086/513501
- Ehlerová, S., Palouš, J., & Huchtmeier, W. K. 2001, *A&A*, 374, 682 doi:10.1051/0004-6361:20010737
- Ehlerová, S., & Palouš, J. 2005, *A&A*, 437, 101
 doi:10.1051/0004-6361:20034389
- Ehlerová, S., & Palouš, J. 2013, *A&A*, 550, AA23
 doi:10.1051/0004-6361/201220341
- Ferrière, K. 2001, *Rev. Mod. Phys.*, 73, 1031
 doi:10.1103/RevModPhys.73.1031
- Gooch, R. 1996, *Astronomical Data Analysis Software and Systems V*, 101, 80 ADS:1996ASPC...101...80G
- Hartmann, D., & Burton, W. B. 1997, *Atlas of Galactic Neutral Hydrogen*, (Cambridge, UK: Cambridge University Press)
 ADS:1997agmh.book.....H
- Heiles, C. 1979, *ApJ*, 229, 533 doi:10.1086/156986
- Heiles, C. 1984, *ApJS*, 55, 585 doi:10.1086/190970
- Hu, E. M. 1981, *ApJ*, 248, 119 doi:10.1086/159135
- Kalberla, P. M. W., Burton, W. B., Hartmann, D., et al. 2005, *A&A*, 440, 775 doi:10.1051/0004-6361:20041864
- Korpela, E. J., Demorest, P., Heien, E., Heiles, C., & Werthimer, D. 2002, in *ASP Conf. Ser.* 276, *Seeing Through the Dust: The Detection of HI and the Exploration of the ISM in Galaxies*, ed. A.R. Taylor, T.L. Landecker, & A.G. Willis (San Francisco, CA: ASP), 100 ADS:2002ASPC...276...100K
- Korpela, E. J., Demorest, P., Heien, E., Heiles, C., & Werthimer, D. 2004, *How Does the Galaxy Work?*, 315, 97
 doi:10.1007/1-4020-2620-X_18
- Mashchenko, S. Y., Thilker, D. A., & Braun, R. 1999, *A&A*, 343, 352 ADS:1999A&A...343...352M
- Mashchenko, S., & St-Louis, N. 2002, *Interacting Winds from Massive Stars*, 260, 65 ADS:2002ASPC...260...65M
- McClure-Griffiths, N. M., Dickey, J. M., Gaensler, B. M., & Green, A. J. 2002, *ApJ*, 578, 176 doi:10.1086/342470
- McGlynn, T., Scollick, K., White, N., 1998, in *IAU Symposium No. 179: New Horizons from Multi-Wavelength Sky Surveys*, ed. B.J. McLean et al. (Kluwer Academic Publishers), 465
 ADS:1998IAUS...179...465M
- McKee, C. F., & Ostriker, J. P. 1977, *ApJ*, 218, 148
 doi:10.1086/155667
- Nishikida, K. 1999, Ph.D. Thesis, Penn. State
 ADS:1999PhDT.....4N
- Peek, J. E. G., Heiles, C., Douglas, K. A., et al. 2011, *ApJS*, 194, 20 doi:10.1088/0067-0049/194/2/20
- Shapiro, P. R., & Field, G. B. 1976, *ApJ*, 205, 762
 doi:10.1086/154332
- Slavin, J. D., & Cox, D. P. 1992, *ApJ*, 392, 131
 doi:10.1086/171412
- Slavin, J. D., & Cox, D. P. 1993, *ApJ*, 417, 187
 doi:10.1086/173302
- Snowden, S. L., Egger, R., Freyberg, M. J., et al. 1997, *ApJ*, 485, 125 doi:10.1086/304399
- Spitzer, L. 1978, *Physical Processes in the Interstellar Medium* (New York, NY: Wiley-Interscience)
 ADS:1978ppim.book.....S
- Suad, L. A., Caiafa, C. F., Arnal, E. M., & Cichowolski, S. 2014, *A&A*, 564, AA116 doi:10.1051/0004-6361/201323147
- Stil, J. M., Taylor, A. R., Dickey, J. M., et al. 2006, *AJ*, 132, 1158
 doi:10.1086/505940
- Thornton, K., Gaudlitz, M., Janka, H.-T., & Steinmetz, M. 1998, *ApJ*, 500, 95 doi:10.1086/305704
- Werthimer, D., Bowyer, S., Ng, D., et al. 1997, *IAU Colloq.* 161: *Astronomical and Biochemical Origins and the Search for Life in the Universe*, 683 ADS:1997abos.conf..683W
- Wenger, M., Ochsenbein, F., Egret, D., et al. 2000, *A&AS*, 143, 9
 doi:10.1051/aas:2000332
- Wolfire, M. G., McKee, C. F., Hollenbach, D., & Tielens, A. G. G. M. 2003, *ApJ*, 587, 278 doi:10.1086/368016
- Xu, Y., Reid, M. J., Zheng, X. W., & Menten, K. M. 2006, *Science*, 311, 54 doi:10.1126/science.1120914

Table 2
Catalog of SETHi Shells

Shell ID	RA (hh mm)	Dec (°)	V_{ref} (km s ⁻¹)	ΔRA (°)	ΔDec (°)	V_1 (km s ⁻¹)	V_2 (km s ⁻¹)	$\Delta\theta$ (°)	S	Q	Q_{exp}	Comment
GSH 029+34+005	16 42	12.25	5	2	1.75	0	12	1.8	0.81	7.9	1.7	
GSH 029+38+005	16 28	13.75	5	4	2.75	2	6	3.1	0.76	8.0	1.7	
GSH 030+67-006	14 33	23.5	-6	2.75	4	-9	-1	3.2	0.72	7.0	2.0	
GSH 034+20+011	17 42	9.5	11	3.5	2.5	8	19	2.8	0.71	6.0	2.3	
GSH 035+36+005	16 42	16.75	5	5.75	5	2	11	4.8	0.85	6.2	3.0	
GSH 039+49-017	15 52	24.25	-17	9	8	-23	-12	8.1	0.96	7.0	2.3	
GSH 040+04+048	18 49	8.25	48	1.75	1.75	39	54	1.7	0.85	7.5	5.8	
GSH 042+21+019	17 50	17	19	13.25	11.5	12	25	12.8	0.70	8.4	1.7	*
GSH 044+00-025	19 11	9.75	-25	1.25	1.5	-31	-18	1.1	0.66	7.1	5.5	
GSH 044+38+002	16 45	24.75	2	2	2.5	-1	5	1.8	0.78	9.5	1.0	
GSH 045+14+031	18 23	17	31	2	2.75	28	39	2.4	0.66	6.4	4.0	
GSH 048-05+045	19 36	11.25	45	6.75	4.5	40	51	4.9	0.64	6.4	4.7	*
GSH 049+08+026	18 51	18.5	26	2.50	2.5	23	29	2.5	0.96	6.2	3.0	*
GSH 052-05+023	19 45	14	23	8	8.25	17	39	7.5	0.85	7.5	6.3	*
GSH 052+01+012	19 26	17.5	12	6.5	5.25	11	16	5.2	0.81	6.5	2.0	
GSH 052+02-071	19 19	17.75	-71	4.75	4.25	-77	-63	4.4	0.86	7.3	1.8	
GSH 052+10-087	18 48	21.25	-87	1	0.75	-91	-82	1.0	0.95	8.7	6.0	
GSH 052+20+012	18 10	25	12	3.75	3	9	17	2.7	0.77	7.8	5.2	
GSH 054-00+003	19 31	18.25	3	1.5	1.5	-1	6	1.4	0.84	7.1	5.8	
GSH 054+01+031	19 27	19	31	2	1.75	28	37	1.7	0.99	8.5	6.5	
GSH 055+18-005	18 20	27.25	-5	6	4	-9	-3	4.5	0.82	7.6	0.7	
GSH 056-06+033	19 57	18	33	3.75	3	23	43	3.0	0.66	6.4	3.3	*
GSH 056+02-074	19 28	21.75	-74	1.4	1.5	-77	-62	1.4	0.70	6.9	6.8	*
GSH 057+04+005	19 24	23.25	5	6.25	6.5	2	9	5.9	0.92	7.2	1.7	*
GSH 057+12-077	18 50	26.5	-77	1.75	1.25	-80	-68	1.1	0.85	8.3	5.3	
GSH 060+01-076	19 40	24.5	-76	3.5	2.5	-80	-68	2.7	0.83	7.2	4.0	
GSH 061-01+000	19 50.5	23.75	0	1.5	1.5	-9	6	1.4	0.82	7.9	3.7	
GSH 062+00+045	19 48	25.25	45	3.5	3.5	37	50	2.7	0.68	6.6	2.7	*
GSH 062+03-102	19 35	27	-102	2	1.75	-107	-99	1.5	0.86	7.8	3.0	
GSH 063+00-022	19 49	26.5	-22	2.25	3	-25	-18	2.3	0.67	8.4	3.7	*
GSH 064-24+011	21 18	13.5	11	3.5	4.5	3	14	3.8	0.79	7.6	2.5	*
GSH 072-30+017	21 56	15	17	2.75	3.25	14	25	3.1	0.83	7.4	1.3	
GSH 080-22+002	21 52	25.5	2	9.25	9.5	-5	8	7.7	0.85	7.8	1.2	
GSH 109-35-011	00 01	26.25	-11	6.75	4.5	-15	-6	4.9	0.55	6.2	1.8	
GSH 110-35-034	00 05.5	26.5	-34	3.25	> 5	-43	-28	4.0	0.75	7.7	6.7	
GSH 112-46-008	00 19	16.25	-8	3.9	5	-14	-5	4.4	0.87	5.6	1.0	
GSH 113-54-005	00 29	8.5	-5	3.25	3	-9	0	2.8	0.74	7.8	6.7	
GSH 116-49-006	00 34	13.5	-6	3.25	3	-9	-5	2.7	0.75	7.9	0.7	
GSH 124-52-008	00 53	10.5	-8	2.75	2.75	-14	-5	2.7	0.86	6.0	2.3	
GSH 134-43-062	01 26	19.5	-62	11.75	9	-68	-51	8.4	0.74	4.5	0.3	*
GSH 139-37+006	01 46	24	6	5.25	4.5	3	11	4.3	0.81	8.2	2.5	
GSH 155-32+005	02 47	23.5	5	6.25	6	3	9	5.0	0.90	7.5	3.0	*
GSH 156-37-003	02 43	19	-3	6.25	4.5	-6	0	4.6	0.67	7.4	3.3	*
GSH 157-27-045	03 05	26.5	-45	6	3.75	-54	-31	4.4	0.75	6.7	1.3	*
GSH 170-21+020	04 06	23.75	20	5.5	4	14	25	4.1	0.91	8.0	3.0	
GSH 179-24+012	04 17	15.5	12	20.75	11.75	11	14	15.9	0.72	9.1	3.3	
GSH 180-31+020	04 00	10	20	4.25	3.5	16	25	3.8	0.98	6.3	4.5	*
GSH 182-18+005	04 46	17.5	5	4.25	3.75	3	9	3.8	0.96	9.4	2.0	
GSH 183-16-031	04 55	18	-31	10.25	11	-37	-20	10.3	0.92	6.4	0.7	
GSH 185-07-009	05 31	20.5	-9	4.25	5.25	-18	-3	4.2	0.65	7.0	2.0	
GSH 187-12+012	05 18	16.5	12	9.25	9.75	9	19	9.1	0.93	8.1	2.0	
GSH 187+01+020	06 05	23	20	3	3	16	26	2.9	0.81	8.3	2.7	
GSH 188+07-079	06 31	25.5	-79	3	6.25	-88	-73	4.5	0.51	4.6	2.7	
GSH 190-02+025	05 59	19.25	25	2	2.25	23	31	2.2	0.83	7.1	0.7	
GSH 192+06-017	06 33	21	-17	3.75	4	-28	-6	3.6	0.86	8.5	1.0	*
GSH 193-01+026	06 09	17.25	26	1.75	1.25	3	31	1.3	0.76	7.1	5.3	
GSH 196+10+008	06 57	19	8	5.75	5	6	12	5.0	0.88	7.5	1.3	
GSH 197-02+034	06 16	13	34	2.75	2.75	31	45	2.5	0.68	6.2	0.8	*
GSH 197+00+002	06 23	14.5	2	3	2	-3	5	2.7	0.78	7.2	1.0	
GSH 198+01+034	06 25	13.75	34	2.75	4.75	29	39	3.2	0.44	6.3	2.8	*
GSH 198+03-018	06 33	14.5	-18	2.5	1.25	-20	-12	1.8	0.68	6.7	3.5	
GSH 200+01-015	06 30	11.75	-15	1.75	2	-20	-8	1.7	0.77	7.6	1.7	
GSH 208+32+006	08 43	18	6	7.75	4.5	2	17	5.5	0.67	6.8	4.0	
GSH 210+54-003	10 12	23.25	-3	3.5	3.5	-9	2	2.6	0.65	7.2	3.0	
GSH 213+28+012	08 34	12	12	4.25	3.25	8	20	3.7	0.77	5.9	0.0	
GSH 221+60+000	10 45	19.25	0	3.5	2.75	-3	3	2.6	0.85	7.4	2.7	
GSH 225+55-005	10 30	15.5	-5	3.25	3.25	-9	-1	3.4	0.92	6.8	0.8	
GSH 228+80-040	12 08	24	-40	7.75	8.5	-48	-29	7.8	0.94	7.8	5.0	
GSH 231+55-009	10 36	12.5	-9	3.75	3	-12	-6	3.0	0.71	6.8	0.0	
GSH 236+75-008	11 51.5	20.25	-8	1.75	1.5	-12	-3	1.1	0.94	8.0	1.0	
GSH 261+74-025	12 08	15	-25	11	5.25	-29	-20	8.0	0.63	7.7	3.3	*
GSH 262+73+003	12 05	13.5	3	11.5	7	2	8	8.6	0.56	7.3	1.0	
GSH 274+74-006	12 19	12.5	-6	10	3.5	-14	-3	5.4	0.52	4.9	0.3	
GSH 294+76+000	12 43	13.25	0	4.5	5.5	-1	8	4.3	0.72	5.4	3.2	

Table 3
Physical Characteristics

Shell ID	l ($^{\circ}$)	b ($^{\circ}$)	D_{ref} (kpc)	D_{min} (kpc)	D_{max} (kpc)	S_{ref} (pc)	S_{min} (pc)	S_{max} (pc)	$D_{\text{ref}2}$ (kpc)	$D_{\text{min}2}$ (kpc)	$D_{\text{max}2}$ (kpc)	$S_{\text{ref}2}$ (pc)	$S_{\text{min}2}$ (pc)	$S_{\text{max}2}$ (pc)	Comment
GSH 040+04+048	40.01	4.29	3.3	2.7	3.9	98	80	120	9.8	9.2	10	290	270	300	
GSH 044+00-025	43.83	0.14	15	14	15	290	270	290	-	-	-	-	-	-	
GSH 045+14+031	45.19	13.81	2.3	1.8	2.8	96	75	120	10	9.6	11	420	400	460	^c
GSH 048-05+045	48.05	-4.57	3.5	2.9	4.2	300	250	360	7.9	7.2	8.5	680	620	730	^{ad}
GSH 049+08+026	49.47	8.41	1.9	1.6	2.3	83	70	100	9.2	8.9	9.6	400	390	420	
GSH 052-05+023	51.54	-5.14	1.7	0.75	2.8	220	98	370	8.9	7.8	9.9	1200	1000	1300	^{ad}
GSH 052+01+012	52.38	0.55	0.81	0.55	1.1	74	50	100	9.6	9.3	9.8	870	840	890	^b
GSH 052+02-071	51.82	2.14	19	17	20	1500	1300	1500	-	-	-	-	-	-	
GSH 052+10-087	51.67	10.24	22	21	24	380	370	420	-	-	-	-	-	-	^{cf}
GSH 054-00+003	53.61	-0.14	0.05	-	0.43	1.2	-	11	10	9.7	10	240	240	240	^g
GSH 054+01+031	53.81	1.05	2.5	2	3.2	74	59	95	7.5	6.9	8.1	220	200	240	^a
GSH 056-06+033	56.47	-5.62	3.1	1.8	-	160	94	-	6.4	-	7.7	340	-	400	^h
GSH 056+02-074	56.34	2.16	18	16	19	440	390	460	-	-	-	-	-	-	^d
GSH 057+04+005	57.23	3.68	0.18	-	0.59	19	-	61	9.1	8.6	9.5	940	890	980	^a
GSH 057+12-077	56.72	12.03	19	18	20	360	350	380	-	-	-	-	-	-	^{cd}
GSH 060+01-076	60.09	1.08	17	16	18	800	750	850	-	-	-	-	-	-	^d
GSH 061-01+000	60.64	-1.37	-	-	0.55	-	-	13	8.6	7.8	9.4	210	190	230	^b
GSH 062+03-102	61.72	3.28	21	20	22	550	520	580	-	-	-	-	-	-	^{di}
GSH 063+00-022	62.84	0.32	10	9.7	10	400	390	400	-	-	-	-	-	-	^d
GSH 187-12+012	187.1	-12.05	8.4	3.5	20	1300	560	3200	
GSH 187+01+020	187.32	0.76	24	9.3	-	1200	470	-	^e
GSH 190-02+025	189.89	-2.31	18	11	33	690	420	1300	^e
GSH 193-01+026	192.8	-1.22	11	3	-	250	68	-	^e
GSH 196+10+008	196.47	9.72	1.5	0.79	2.4	130	69	210	^{cd}
GSH 197-02+034	197.34	-1.78	10	6.4	17	440	280	740	^e
GSH 197+00+002	196.82	0.43	0.38	-	1.2	18	-	57	
GSH 198+01+034	197.71	0.51	9.8	7.2	14	550	400	780	^e

^a Greater distance more likely based on Galactic spiral structure in direction of shell

^b Greater distance somewhat preferred based on Galactic spiral structure and/or shell size

^c Not clear if shell is associated with local or Galactic gas. Kinematic distances could well be inaccurate.

^d Inferred shell size plausible in context of extent of Galactic plane

^e Seems associated with spiral structure but kinematic distances are too large for spiral structure in this direction (actually at 2.5 kpc not 10 kpc). May be affected dramatically by streaming motions. Kinematic distances could well be inaccurate.

^f Fairly high above Galactic plane given the kinematic distance. Kinematic distances could well be inaccurate.

^g Appears to be in the nearer of 2 spiral arms. Likely the larger distance because a shell < 10 pc in size is unlikely if embedded in a spiral arm.

^h Allowed distance ranges for the two solutions overlap. Likely nearer the upper edge of range based on spiral arm locations in this direction.

ⁱ Appears to be part of 3rd spiral arm along line of sight (recently discovered to extend in this direction).

Table 4
Expansion Velocities

Shell ID	Q_{exp}	V_f (km s ⁻¹)	V_b (km s ⁻¹)	V_{exp} (km s ⁻¹)	V_1 (km s ⁻¹)	V_2 (km s ⁻¹)	LL on V_{exp} (km s ⁻¹)	Comment
GSH 040+04+048	5.8	33	39	54	11	d
GSH 044+00-025	5.5	-43	-12	16	-31	-18	13	cd
GSH 045+14+031	4.0	17	40	12	28	39	6	abf
GSH 052-05+023	6.3	10	50	20	17	39	15	cde
GSH 052+10-087	6.0	...	-77	...	-91	-82	7	b
GSH 052+20+012	5.2	0	20	10	9	17	9	acd
GSH 054-00+003	5.8	-8	9	9	-1	6	...	
GSH 054+01+031	6.5	23	42	10	28	37	7	abce
GSH 056+02-074	6.8	-80	-57	12	-77	-62	9	cd
GSH 057+12-077	5.3	...	-53	...	-80	-68	14	bfg
GSH 193-01+026	5.3	-5	3	31	18	dh
GSH 228+80-040	5.0	-56	-48	-29	14	de

a Front wall estimate may be possibly unrelated gas, or suffer from data quality issues.

b Estimated V_{exp} lower limit uses V_1 and V_b .

c Rear wall estimate may be possibly unrelated gas, or suffer from data quality issues.

d Estimated V_{exp} lower limit uses V_f and V_2 .

e Based on raw spectrum.

f Expansion velocity might be underestimated because at least one maximum in spectrum is broad and/or peaks at a velocity very close to last shell-like velocity.

g Clear maximum on one side, but no clear minimum in spectrum.

h Spectrum complex, and constantly changing histogram limits required to follow its morphology vs. velocity.

Table 5
Derived Shell Properties

Shell ID	t_1 (Myr)	$E_1 P^{-1}_{3000\text{cm}^{-3}\text{K}}$ (erg)	$E_{K1} n^{-1}_{\text{cm}^{-3}}$ (erg)	$E_{\text{Ch1}} n^{-1.12}_{\text{cm}^{-3}}$ (erg)	t_2 (Myr)	$E_2 P^{-1}_{3000\text{cm}^{-3}\text{K}}$ (erg)	$E_{K2} n^{-1}_{\text{cm}^{-3}}$ (erg)	$E_{\text{Ch2}} n^{-1.12}_{\text{cm}^{-3}}$ (erg)	Comment
GSH 040+04+048	4.3	8.7×10^{48}	13.	2.3×10^{50}	a
GSH 044+00-025	8.6	2.1×10^{50}	1.0×10^{51}	1.3×10^{52}	
GSH 045+14+031	3.9	8.5×10^{48}	2.3×10^{49}	3.0×10^{50}	17.	7.1×10^{50}	1.9×10^{51}	3.0×10^{52}	b
GSH 048-05+045	...	2.5×10^{50}	3.0×10^{51}	c
GSH 049+08+026	...	5.9×10^{48}	6.3×10^{50}	
GSH 052-05+023	5.5	1.1×10^{50}	8.1×10^{50}	8.7×10^{51}	29.	1.5×10^{52}	1.1×10^{53}	1.5×10^{54}	c
GSH 052+01+012	...	3.9×10^{48}	6.3×10^{51}	c
GSH 052+02-071	...	2.8×10^{52}	
GSH 052+10-087	27.	5.8×10^{50}	ab
GSH 054-00+003	0.054	9.6×10^{42}	1.5×10^{43}	1.3×10^{44}	13.	1.4×10^{50}	2.1×10^{50}	3.8×10^{51}	c
GSH 054+01+031	3.7	4.0×10^{48}	7.6×10^{48}	1.1×10^{50}	11.	1.1×10^{50}	2.0×10^{50}	3.2×10^{51}	c
GSH 056-06+033	...	3.9×10^{49}	3.6×10^{50}	c
GSH 056+02-074	18.	7.8×10^{50}	2.1×10^{51}	3.3×10^{52}	
GSH 057+04+005	...	6.6×10^{46}	7.7×10^{51}	c
GSH 057+12-077	13.	4.5×10^{50}	ab
GSH 060+01-076	...	4.8×10^{51}	
GSH 061-01+000	8.9×10^{49}	cd
GSH 062+03-102	...	1.7×10^{51}	
GSH 063+00-022	...	6.3×10^{50}	
GSH 187-12+012	...	2.3×10^{52}	
GSH 187+01+020	...	1.7×10^{52}	b
GSH 190-02+025	...	3.1×10^{51}	b
GSH 193-01+026	6.8	1.5×10^{50}	ab
GSH 196+10+008	...	2.2×10^{49}	b
GSH 197-02+034	...	8.6×10^{50}	b
GSH 197+00+002	...	5.6×10^{46}	
GSH 198+01+034	...	1.6×10^{51}	b

a Expansion velocity lower limit used to derive age limits.

b Treat results with caution, as kinematic distances may be inaccurate.

c Greater age limits and/or energies preferred, based on kinematic distance preference noted earlier.

d Smaller kinematic distance option only gave an upper limit on distance.

Table 6
Shell Axes and Position Angles

Shell ID	a ($^{\circ}$)	b ($^{\circ}$)	ϕ ($^{\circ}$)
GSH 029+34+005	1.1	0.7	139
GSH 029+38+005	1.9	1.2	134
GSH 030+67-006	2.0	1.1	173
GSH 034+20+011	1.8	1.0	89
GSH 035+36+005	2.7	2.0	137
GSH 039+49-017	4.2	3.9	125
GSH 040+04+048	1.0	0.7	138
GSH 042+21+019	8.3	4.5	155
GSH 044+00-025	0.7	0.4	174
GSH 044+38+002	1.1	0.7	2
GSH 045+14+031	1.6	0.8	174
GSH 048-05+045	3.3	1.6	105
GSH 049+08+026	1.3	1.2	71
GSH 052+01+012	3.1	2.1	104
GSH 052+02-071	2.5	1.9	81
GSH 052+10-087	0.5	0.5	139
GSH 052+20+012	1.7	1.0	144
GSH 052-05+023	4.3	3.2	7
GSH 054+01+031	0.9	0.8	79
GSH 054-00+003	0.8	0.6	5
GSH 055+18-005	2.7	1.8	125
GSH 056+02-074	0.9	0.5	170
GSH 056-06+033	2.0	1.0	82
GSH 057+04+005	3.2	2.7	40
GSH 057+12-077	0.7	0.5	132
GSH 060+01-076	1.5	1.1	125
GSH 061-01+000	0.8	0.6	173
GSH 062+00+045	1.8	0.9	56
GSH 062+03-102	0.9	0.7	172
GSH 063+00-022	1.5	0.8	6
GSH 064-24+011	2.3	1.5	11
GSH 072-30+017	1.8	1.3	58
GSH 080-22+002	4.4	3.2	69
GSH 109-35-011	3.5	1.3	131
GSH 110-35-034	2.5	1.5	84
GSH 112-46-008	2.5	1.9	69
GSH 113-54-005	1.8	1.0	100
GSH 116-49-006	1.6	1.0	174
GSH 124-52-008	1.5	1.2	92
GSH 134-43-062	5.3	3.1	17
GSH 139-37+006	2.5	1.7	43
GSH 155-32+005	2.8	2.3	13
GSH 156-37-003	3.1	1.5	51
GSH 157-27-045	2.7	1.6	60
GSH 170-21+020	2.2	1.9	44
GSH 179-24+012	10.2	5.7	50
GSH 180-31+020	1.9	1.9	48
GSH 182-18+005	2.0	1.8	144
GSH 183-16-031	5.6	4.7	149
GSH 185-07-009	2.8	1.4	175
GSH 187+01+020	1.7	1.2	180
GSH 187-12+012	4.9	4.2	144
GSH 188+07-079	3.4	1.1	148
GSH 190-02+025	1.3	0.9	170
GSH 192+06-017	2.1	1.6	167
GSH 193-01+026	0.8	0.5	61
GSH 196+10+008	2.8	2.2	87
GSH 197+00+002	1.6	1.0	42
GSH 197-02+034	1.6	0.8	15
GSH 198+01+034	2.5	0.7	173
GSH 198+03-018	1.2	0.6	63
GSH 200+01-015	1.0	0.6	166
GSH 208+32+006	3.7	1.9	58
GSH 210+54-003	1.7	0.8	120
GSH 213+28+012	2.3	1.4	40
GSH 221+60+000	1.5	1.1	95
GSH 225+55-005	1.8	1.5	74
GSH 228+80-040	4.2	3.7	3
GSH 231+55-009	1.9	1.1	50
GSH 236+75-008	0.6	0.5	155
GSH 261+74-025	5.6	2.6	41
GSH 262+73+003	6.3	2.4	52
GSH 274+74-006	4.0	1.4	29
GSH 294+76+000	2.8	1.6	126